3

Low speed laser welding of aluminium alloys using single-mode fiber lasers

Jay F. Tu and Alexander G. Paleocrassas
North Carolina State University
USA

1. Introduction

Laser welding of aluminium alloys is an important industrial technology and yet many challenges still lie ahead. Laser welding studies were reported almost within two years since the first laser was invented in 1960. However, practical metal seam welding was not feasible until the early 1970s when multi-kilowatt, continuous wave CO_2 lasers were developed to allow for deep penetration keyhole welding (Duley, 1999). Unfortunately, the application for deep penetration welding of aluminium was limited due to its very high reflectivity at the relatively long wavelength (10.6 micron) of CO_2 lasers. Flash-pumped Nd:YAG lasers with a 1.06 micron wavelength were not suitable due to their low power and extremely poor efficiency at the time. Since the 1980s, high power seam welding of carbon steels using multi-kilowatt CO_2 lasers has become a regular industrial practice, in particular in the automotive industry. In the mid 1990s, diode pumped Nd:YAG lasers were developed that offered kilowatt power and high efficiency. As a result, aluminium laser welding became more feasible because the beam absorption of aluminium alloys at 1.06 micron is three times as much as it is at 10.6 micron. Nevertheless, the poor beam quality and high cost of diode-pumped Nd:YAG lasers still hinders their acceptance in industry. In the early 2000s, with the arrival of single-mode and multi-mode high power fiber lasers at a 1.075 micron wavelength, along with excellent beam quality and low maintenance cost, the expectation was that the advantage of laser welding aluminium components could be better realized.

The requirement of very high laser power for aluminium welding is not only due to its high reflectivity and high heat conductivity. Aluminium has been known to be one of the most challenging metals to weld successfully (Mandal, 2002). Other factors affecting the weld quality of aluminium alloys include different kinds of porosity formation, hot tearing, solidification cracking, oxide inclusions and loss of alloying elements. It has been found that weld porosities can be significantly suppressed at high welding speeds. In order to maintain a stable keyhole at high speeds, very high laser power is needed. What has been less explored is the reason why the welding process becomes less stable and prone to defects as the speed is reduced. There are many applications where high speed welding is not suitable. With the expansion of modern miniaturized consumer products, the weld path can be short and with intricate shapes. High welding speed may not be effective due to the short paths and constant accelerations and decelerations required to follow the path precisely. One such

application is the fusion of fatigue cracks in aluminium parts, where a crack path is irregular. It also has been shown that welding at a lower processing speed can reduce the tendency of transverse solidification cracking. Finally, with the availability of better laser sources such as high power fiber lasers, it is important to expand laser welding of aluminium to wider processing conditions for various applications.
This book chapter will discuss latest research results in extending laser welding of aluminium in the low speed range by investigating the welding instability phenomena. The following topics will be discussed:

- Aluminium alloys and welding defects
- Brief review of high speed laser welding of aluminium
- High power fiber lasers and optical setups
- Process modelling of laser welding of aluminium
- Experimental process characterization of low speed welding
- The instability and defects at low speed welding
- Applications of fatigue crack repair in aluminium

First, the properties of aluminium alloys and the cause of welding defects are discussed. Prior to discussing low speed welding, a brief review of high speed laser welding of aluminium is provided. The characteristics of high power fiber lasers and their optical setups for welding applications, such as focusing lens, assist gas, alignments, and damage prevention due to beam reflection by aluminium are then presented. The chapter then proceeds to present recent research results in low speed laser welding of aluminium, which includes theoretical process modelling, experimental process characterization, in-process monitoring of several critical signals, such as plasma radiation and beam reflection, as well as the causes and consequences of process instability at low speeds. The transition of process stability from medium welding to a low speed threshold and its mechanisms are explored. Finally, an application of low speed laser welding of aluminium for fatigue crack repair is given. A discussion on different applications and future development conclude the chapter.

2. Background and Reviews

2.1 Aluminium Alloys

Aluminium alloys can be separated into two major categories: Non heat-treatable and heat-treatable. The initial strength of non heat-treatable alloys depends primarily upon the hardening effect of alloying elements such as silicon, iron, manganese and magnesium. The non heat-treatable alloys are mainly found in 1xxx, 3xxx, 4xxx and 5xxx series. Additional strength is usually achieved by solid-solution strengthening or strain hardening.
The initial strength of heat-treatable alloys depends upon the alloy composition, just like the non heat-treatable alloys. In order to improve their mechanical properties they need to undergo solution heat treating and quenching followed by either natural or artificial aging (precipitation hardening). This treatment involves maintaining the work piece at an elevated temperature, followed by controlled cooling in order to achieve maximum hardening. The heat-treatable alloys are found primarily in the 2xxx, 6xxx and 7xxx alloy series (ibid).
The 7xxx series alloys contain zinc in amounts between 4 and 8 % and magnesium in amounts between 1 and 3 %. Both have high solid solubility in aluminium. The addition of

magnesium produces a marked increase in precipitation hardening characteristics. Copper additions between 1 and 2 % increase the strength by solid solution hardening, and form the basis of high strength aircraft alloys. The addition of chromium, typically up to 0.3 %, improves stress corrosion cracking resistance. The 7xxx series alloys are predominantly used in aerospace applications, 7075-T6 being the principal high strength aircraft alloy (Ion, 2000). This chapter will focus on fiber laser welding of 7075-T6 because of its predominant use in aircraft components.

2.2 Laser Welding Defects in Aluminium

Laser welding is one of the most promising metal joining methods because it can provide high productivity, high weld quality, high welding speed, high weld aspect ratio, low heat input, low distortion, manufacturing flexibility and ease of automation (Duley, 1999, Mandal, 2002). According to a study on phase transformations in weldments (Cieslak, 1992), solidification rates of 10^2 to 10^3 ^oC/sec encountered in conventional arc welding processes, are much lower compared to high-energy density laser processes which reach 10^5 to 10^6 ^oC/sec as a result of high heat input experienced at high travel speeds. Under these processing conditions the weld metal microstructure bears no resemblance to that expected as the result of arc welding. Consequently, the weldment is mostly comprised by fine-grained microstructures.

There are four major types of weld defects in laser welding of aluminium: a) porosity, b) cracking, c) inclusions and d) loss of alloying elements (Matsunawa, 1994, Cao, *et al.*, 2003).

Hydrogen porosity: Hydrogen is very soluble in aluminium and its alloys. Most gas porosities precipitated in aluminium alloys are attributed to hydrogen. The solubility of hydrogen in liquid aluminium is an exponential function of temperature, which is why its porosity is a much bigger problem in laser welding (than in conventional welding) due to increased temperatures. Also, the high cooling rate is very unfavorable because it does not allow for diffusion (i.e. "floatation") of the trapped hydrogen. Normal hydrogen levels in molten aluminium vary from approximately 0.10 to 0.40 mL/100g. It is worth noting here that in order for an aircraft part to pass aerospace quality inspections, the gas contents have to be less than 0.06 mL/100g. A critical lower welding speed possibly exists at which formation and growth of hydrogen porosity can be prevented. Also, another way to reduce hydrogen porosity is to increase power density, because it keeps the keyhole stable and increases solidification time, allowing the hydrogen to escape (Cao, *et al.*, 2003).

According to a study conducted on porosity formation (Kutsuna and Yan, 1998), the rate of hydrogen porosity shows a tendency to rise considerably as the magnesium content increases. This happens because magnesium in aluminium alloys raises the hydrogen solubility in the molten pool and hence the segregation of magnesium enhances the segregation of hydrogen during solidification.

Porosity caused by collapse of unstable keyholes: Even with proper material surface preparation, laser parameters, shielding gas and material compositions, aluminium alloys are susceptible to random porosities after laser welding (Weeter, 1998). Keyhole instability and the coupling of the laser beam into the metal are suspected to cause these random events. These porosities have irregular or turbular form and are large enough to be visible with x-ray analysis (Dausinger, *et al.*, 1997). They are usually located in the keyhole path, whereas hydrogen pores are more or less equally distributed with slight enrichment at the melting line. The number of cavities is strongly influenced by processing parameters such as the

power, focusing and wavelength. Most likely, keyhole stability is increased with the shorter wavelength lasers (Nd:YAG) because the beams are not as drastically affected by the weld plume as the ones with longer wavelength lasers (CO_2). In the latter case, the weld plume periodically blocks the beam from impinging on the metal and thus causes an instability in the keyhole. The shorter wavelength laser beams can pass through the plume and can provide a more consistent heat input into the metal (Weeter, 1998). It has also been observed that the highest level of porosity is concentrated in the regions where an unstable keyhole is formed. They are mainly composed of metal vapor but will condense at room temperature. The way to reduce this type of porosity is to keep the keyhole as stable as possible; this can be achieved by welding at high speeds and the addition of filler wire. Also, the use of high-power continuous wave (CW) can improve the stability of keyholes (Cao, *et al.*, 2003b).
Results based on a study that was conducted in vacuum and under low pressure welding with a tornado nozzle were reported to reduce or suppress porosity. It was also reported that the forward welding with about 15 to 20 degrees of beam inclination was able to reduce porosity (Katayama, *et al.*, 2003). However, full penetration and pulse-modulated welding approaches were not completely effective.
Cracking: Aluminium alloys exhibit a strong propensity for weldment crack formation because of their large solidification temperature range, high coefficient of thermal expansion, and large solidification shrinkage. The restrained contraction of a weld during cooling, sets up tensile stresses in the joint which may cause cracking. There are two types of hot cracking: a) cracking that occurs in the weld fusion zone during solidification of the weld metal which is known as solidification cracking, and b) cracking that takes place in the primary melting zone due to tearing of the liquate, called liquation cracking (Zhao, *et al.*, 1999). These cracks are detrimental to the integrity of the weld since they form areas of high stress concentration and will significantly reduce the strength of the weld, probably leading to catastrophic failure.
Oxide Inclusions: Oxides are one of the main types of inclusions in aluminium alloys. During keyhole laser welding, the inherently unstable keyhole flow may entrap shielding gas or even air because of imperfect gas shielding (Matsunawa, *et al.*, 1998). Additionally, the shielding gas cannot be truly pure; therefore, some oxide particles may be present in the keyhole vapor. The surface of liquid metal in weld pools (strictly speaking, the surface here should be referred to as the interface between the liquid metal in the weld pool and metal vapor or shielding gas) may also be partly oxidized to form oxide films because of the entrapment of air or shielding gas into the pools. Depending on the magnesium contents in aluminium alloys, oxides such as Al_2O_3, Al_2MgO_4, MgO, or their combination may occur. When aluminium alloys contain magnesium, because it is surface active in liquid aluminium, the oxidizing tendency of the molten aluminium increases rapidly with magnesium contents. When the aluminium alloys contain a trace of magnesium, a mixed oxide ($MgAl_2O_3$), spinel, is formed. When the magnesium content of the alloy exceeds approximately 2%, the liquid oxidizes rapidly to form MgO. The oxides entrained into welded metal because of surface turbulent flow in welding are referred to as young oxides. Oxides in base metal, originally from primary processing of aluminium alloys are termed old oxides.
Loss of Alloying Elements: The high power density used for laser welding may cause selective vaporization of some alloying elements with a low fusion point such as lithium, magnesium, and zinc because of their higher equilibrium vapor pressure than aluminium. Selective

vaporization of alloying elements can take place in both keyhole and conduction mode laser welding. The vaporization mechanism is divided into three stages. The first stage involves transport of vaporization elements from the bulk to the surface of the molten weld pool. Then the vaporization of elements occurs at the liquid/vapor interface, and finally the vaporized species are transported into the surrounding gas phases (Cao, *et al.*, 2003ab). This will also cause a void on the top of the weld called underfill. It was found that the intrinsic vaporization of alloying elements at the weld pool surface, controls the overall vaporization (Zhao, *et al.*, 1999).

The loss of alloying elements can be minimized by controlling the beam power density distribution during continuous wave (CW) laser welding, which can influence the temperature of the molten metal in the welding pool (Cao, *et al.*, 2003ab). Another way of reducing this loss is through the use of filler metal, which is used as an auxiliary source of material to fill the gap. It also provides a means of controlling the metallurgy of the weld bead and ensures weld quality (Ion, *et al.*, 2001), by helping replenish the loss of alloying elements and also prevent solidification cracking. The use of filler metal in laser welding is justified only if the joint gap and sheet metal thickness is larger than the beam and loss of alloying elements is significant (Molian, 2004). Some skepticism remains about the process, mainly because it is considered to be complex and requires high precision. The interactions between the large number of process variables involved are also not fully understood (Ion, *et al.*, 2001).

2.3 High Speed Laser Welding of Aluminium

Dausinger, et al., (1996) reported that with a 2.2 kW Nd:YAG laser, weld depths of up to 3.7 mm in AA 6082 have been obtained at approximately 16.7 mm/s, at a power density of 3 MW/cm^2. Also, Yoshikawa, et al. (1995), report that successful butt welds of 3 mm thick 5 and 6 series aluminium alloys can be obtained. They also used high duty cycle power modulation (pulsing) in order to prevent cracks. In a different study, a 3 kW CO_2 laser has been able to achieve approximately 2.5 mm weld depth in aluminium alloy 7075-T6 at about 25 mm/s (Katayama and Mizutani, 2002). Also, a 4.5 kW CO_2 produced penetration depths of 3.5 mm in aluminium alloy series 5000 (non heat-treatable) and 6000 (heat-treatable), at a speed of approximately 33 mm/s; in comparison, a 4 kW Nd:YAG produced weld depths of 4 mm at the same speed (Cao, et al., 2003a). In addition, Ramasamy and Albright (2000) showed that when welding with a pulsed 2 kW Nd:YAG, or a 3 kW continuous wave Nd:YAG, or a 3-5 kW CO_2 laser, vaporization of magnesium and/or silicon can occur from aluminium alloy 6111-T4 and also the metal hardness was reduced. This means that when operating at very high power densities, loss of alloying elements is a significant problem.

Some other more recent studies are also worth being reviewed. Oi et al. (2006) used a slab CO_2 laser for bead-on-plate and filler wire welding of 2.4 mm thick AA 7075-T6. Mechanical properties of these welds were examined and, after heat treatment, achieved tensile strengths between 75 and 84 percent (depending on the filler metal added) of the base metal. Another study on the mechanical properties of laser welded heat-treatable aluminium was conducted by Xu et al. (2008). They used a CO_2 laser to weld AA 2519-T87 and examined the weld's microstructure and tensile strength. Results showed that the grains in the welds were very fine and the tensile strength, after heat treatment, reached up to 75 percent of the base metal as compared to 61 percent for MIG welding.

2.4 Single-Mode High Power Fiber Lasers

The power source used in this study is a 300 W, Single-Mode, Ytterbium Fiber Optic Laser. The power unit consists of six 50 W modules which are combined to produce an output power of 300 W. Each module contains a fiber optic bundle through which the laser light resonates. The fiber is doped with a rare earth called ytterbium, and acts as the laser gain medium. Each module contains several diode lasers which serve as the pump (IPG, 2003).

	Fiber Laser	Nd:YAG	CO_2	Disc
Wall Plug Efficiency	30%	~ 5%	~ 10%	15%
Output Powers	to 50 kW	to 6kW	to 20 kW	to 4 kW
BPP (4/5kW)	< 2.5	25	6	8
Diode Lifetimes	100,000	10,000	N.A.	10,000
Cooling	Air/Water	Dionized	Water	Water
Floor Space (4/5kW)	< 1 m^2	6 m^2	3 m^2	> 4 m^2
Operating Cost/hour	$21.31	$38.33	$24.27	$35.43
Maintenance	Not Required	Often	Required	Often

Table 1. Characteristics comparisons between major high power industrial lasers (Industrial Laser Solutions, 2005).

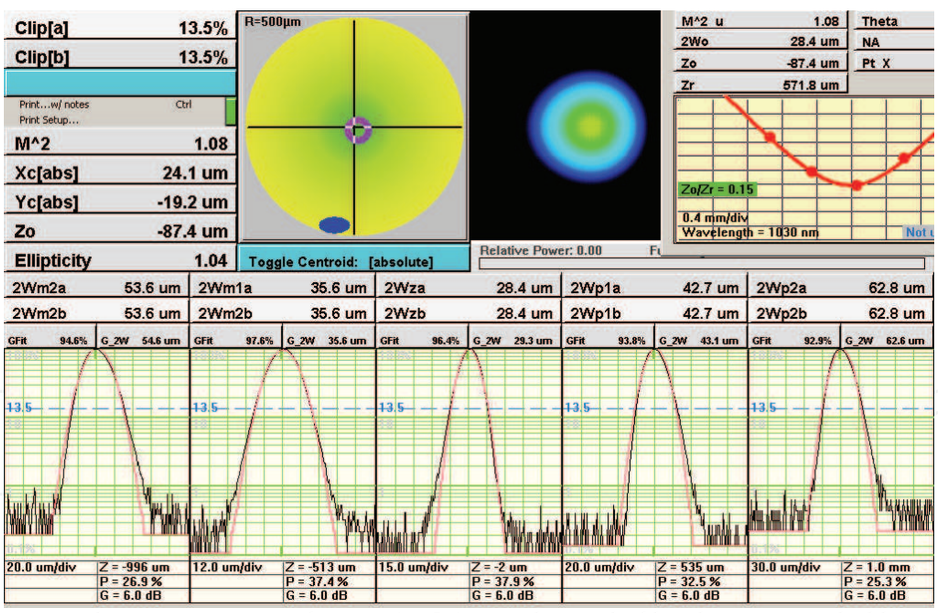

Fig. 1. Beam mode measurement of a 300 W, CW, single-mode fiber laser, provided by IPG, Inc.

A comparison of a high power single-mode fiber laser and other major industrial lasers is listed in Table (1). It is clear that high power fiber lasers have large advantages in wall plug efficiency, maximum output powers, beam quality, reliability and operating cost. Among these advantages, the beam quality, as measured by Beam Parameter Product (BPP) (beam waist radius times divergence angle) and the M^2 value are most impressive. Their M^2 value

of approximately 1.08 (Figure 1) is very close to a Gaussian (normal) power distribution. This allows the beam to be focused to a very small spot to achieve very high power densities. In addition to the excellent beam quality, this laser has a wavelength of approximately 1.075 μm (near infrared spectrum), which is relatively short compared to CO_2 lasers. This allows for increased absorption, useful for welding highly reflective materials like aluminium. The beam diameter exiting the collimator is approximately 7 mm, and can be focused down to about 10 μm. At 300 W, a maximum power density of about 382 MW/cm^2 can be achieved.

2.5 Review of Laser Welding with Single-Mode Fiber Lasers

Limited research has been conducted on laser welding using fiber lasers. Prof. Miyamoto was one of the first to realize the advantages of the fiber laser and propose that it be used in laser welding (Miyamoto, et al., 2003). His experiments were performed on stainless steel foil with a limited output power (~50 W). Ever since, there have been others who have recognized the value of fiber lasers in laser material processing. Allen at al. (2006) used a high power fiber laser as part of a broader study in welding of 7000 series aluminium alloy of thicknesses between 6 and 12 mm. The processing parameters of power and welding speed were not mentioned, however, for proprietary information purposes. Another more recent study (Brown, 2008) focused on keyhole welding on several different metals, including AA 1100, using a moderate power fiber laser (600 W). Uniform high aspect ratio welds were observed, which were in reasonable agreement with the two-dimensional Rosenthal model for a moving-line heat source that was used for comparison. Also, Katayama et al. (2008) used a high power fiber laser to investigate the various welding conditions on penetration and defect formation, on several aluminium alloys and in particular AA5083. Power densities ranged from 40 kW/cm^2 to 90 MW/cm^2. At 64 MW/cm^2 and 10 m/min (166.7 mm/s) 10 mm thick plates were penetrated fully. Porosity was generated at certain processing conditions, reasons for which were given by interpreting the keyhole and molten metal behaviors, observed using a high speed camera and micro-focused X-ray transmission. It was found that nitrogen gas was more effective than argon, in minimizing or even preventing porosities.

Other research using fiber lasers includes a study on micromachining using a 100 W, single mode fiber laser (Naeem and Lewis, 2006). This research group has focused their study on micro joining and micro cutting various metals using both continuous wave and pulsed modes. Similarly, Wagner (2006) studied high speed micro welding of thin sheets of various metals including aluminium, assessing the potentials for low distortion at high speeds. The processing speeds employed reached 100 m/min (1667 mm/s).

2.6 Experimental Setup for Fiber Laser Welding

An optical isolator was attached to the collimator and is used to divert any reflected light away from the collimator in order to avoid damage to the fiber due the high reflectivity of aluminium. Consequently, the beam diameter and beam quality were changed slightly. The beam diameter increased from 5 mm in diameter to 7 mm, while the M^2 value goes from 1.08 to 1.15.

A 3x beam expander is used in combination with the 100.1 mm triplet lens to obtain a minimum focus spot size of 12.0 µm. Equation 1 shows how to calculate the minimum spot size.

$$\text{Spot size} = \frac{\text{Lens Focal Length}}{\text{Collimator Optics Focal Length} * \text{ Beam Expantion Factor}} * \text{Fiber Diameter} = \frac{100.1\text{ mm}}{25\text{ mm} * 3} * 9\ \mu\text{m} = 12.01\ \mu\text{m} \quad (1)$$

The laser beam is centered with respect to the beam expander and the laser head. The laser head contains the focusing triplet and can be adjusted using the outer ring. At the bottom of the cutting head there is a chamber that allows for shielding to flow out through the welding nozzle. This chamber is sealed by a special cover glass and a rubber gasket.
The determination of the laser beam's focusing position was done by using a laser drilling technique. One of the fiber laser's particular characteristics is that when a laser pulse is released, there is an approximately 1,500 W power spike that is output for about 1 µs before it drops to the steady-state power value of 300 W. By pulsing the laser for a very short time, approximately 3 µs, we can take advantage of this power spike and create a very high power density at the focus plane. This enables us to perform laser ablation to form a crater into a stainless steel plate. The focusing technique utilizes this process, by creating spot welds or holes at different z-positions, every 10 µm. A picture is taken of each group of welds/holes and using special calibrated software, the radii are measured and plotted versus the z-focus position.

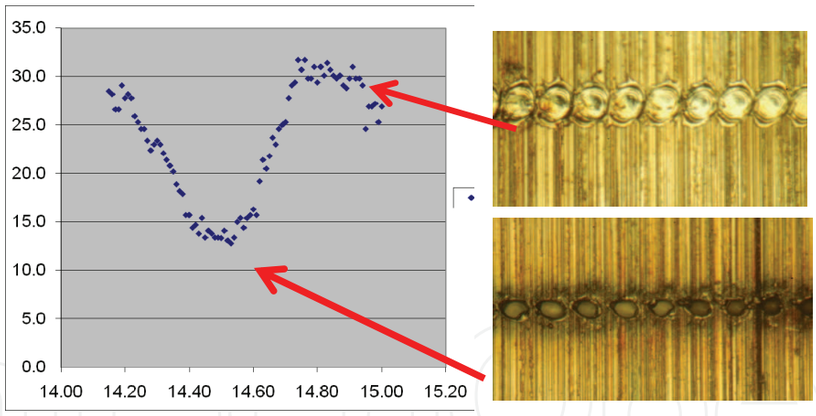

Fig. 2. Spot welds or holes at different focusing locations

Since the laser spot size is very different at different focusing positions, the pulsing will either create very small holes, approximately on the order of the focused beam spot size, or larger spot welds. When all the radii are plotted, the minimum of the resulting curve shows the approximate location of the focusing plane. This is a relatively quick and effective way to find the location of the focus. This technique can be further expanded to obtain the beam profile along its propagation axis (Harp et al, 2008).

3. Low Speed Laser Welding of Aluminium

3.1 Modeling of an Idealized Welding Process

A 2-D heat conduction model for laser welding is reported in Lankalapalli, Tu, and Gartner (1996). This model makes several assumptions which significantly reduce its complexity. The general idea of the model is to calculate the heat conduction over an infinitesimally thin layer of thickness (depth) dz at a specific distance from the top of the surface (Figure 3).

One of the assumptions made, is that the walls of the keyhole within this layer are perpendicular to the surface and that heat conducted in the z-direction is much less than the heat conducted in the radial direction. Therefore, a conical keyhole can be divided into an infinite number of such infinitesimally thin layers and the depth can be approximated by cylindrical heat sources of varying radii, moving together at a constant speed in each of these thin layers. Another assumption made is that there is a quasi-steady state environment in which a cylindrical surface of radius a, at uniform temperature T_V, is moving with a constant speed, v, along the x direction, in an infinite medium initially at constant temperature, T_0. Finally, assuming that the thermal properties of the medium are constant and that the axis of the cylindrical surface passes through the origin of the coordinate system, the governing differential equations and boundary conditions for the temperature distribution can be written as:

$$\frac{\partial^2 T}{\partial x^2} + \frac{\partial^2 T}{\partial y^2} + \frac{v}{\alpha}\frac{\partial T}{\partial x} = 0 \tag{2}$$

$$T = T_V \text{ at } x^2 + y^2 = a^2 \tag{3}$$

$$T(x, y) \to T_0 \text{ as } x \to \pm\infty \text{ and y} \to \pm\infty \tag{4}$$

where x and y are the surface coordinates, z is the depth coordinate, a is the keyhole radius, v is the welding speed, α is the thermal diffusivity, T_0 is the initial temperature and T_V is the vaporization temperature of the material (Carslaw and Jaeger, 1962).

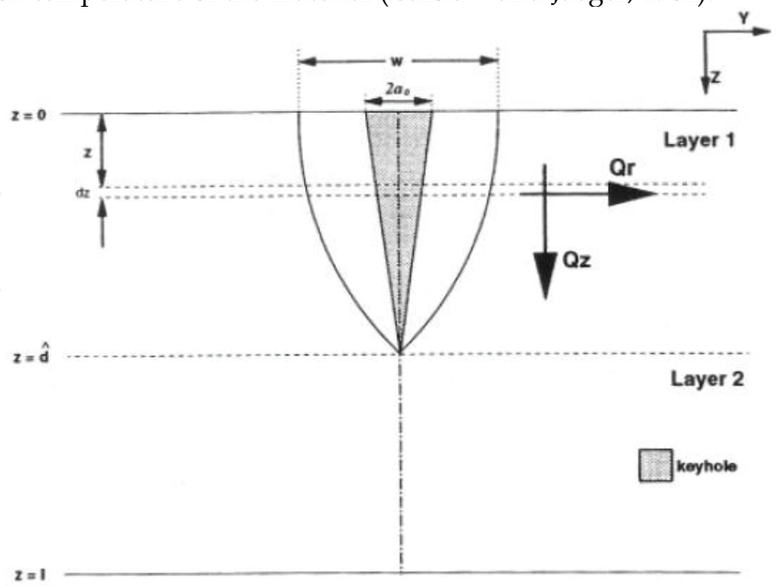

Fig. 3. Keyhole and the resulting weld profile, in which a work piece is sliced to many thin layers (Lankalapalli, Tu, and Gartner, 1996)

After several derivations, the following equation which estimates penetration was found as (Lankalapalli, Tu, and Gartner, 1996)

$$d = \frac{P_i}{k(T_V - T_0)} \frac{1}{\sum_{i=1}^{6} \frac{c_i}{i} (Pe_0)^{i-1}} \tag{5}$$

where k is the thermal conductivity of the material and c_i are coefficients to a polynomial fit to the equation that was evaluated numerically for 100 different values of Pe in the operating range of 0 - 0.025:

$$g(Pe) = \int_0^{2\pi} G(\theta, Pe) d\theta = C_1 + C_2 Pe + C_3 Pe^2 + C_4 Pe^3 + C_5 Pe^4 + C_6 Pe^5 \tag{6}$$

where

$$G(\theta, Pe) = Pe * e^{(\ Pe\cos\theta)} * \sum_{n=0}^{\infty} \varepsilon_n I_n(Pe) \cos(n\theta) \ \frac{n}{Pe} \ \frac{K_{n+1}(Pe)}{K_n(Pe)} \ \cos\theta \tag{7}$$

$$= \frac{}{r^*} \ \frac{T_V \ \ T}{T_V \ \ T_0} \Big|_{r^*=1}$$

$$\frac{T_V - T}{T_V - T_0} = 1 - e^{(-Pe * r^* \cos\theta)} * \sum_{n=0}^{\infty} \varepsilon_n \frac{I_n(Pe)}{K_n(Pe)} K_n(Pe * r^*) \cos(n\theta) \tag{8}$$

is the closed-form solution in polar coordinates (r,θ) of the aforementioned governing differential equation with the specified boundary conditions for the temperature distribution, where Pe = v*a / (2α) is the Péclet number, $r^* = r/a$ is the normalized radial coordinate, $\varepsilon_n = 1$ for n = 0 and 2 for n ≥ 1, I_n is a modified Bessel function of the first kind, of order n and K_n is a modified Bessel function of the second kind of order n. Note that the above model is not material specific. With proper material parameters and process parameters incorporated, this model allows for very rapid simulation of the temperature field at the top surface (Equation 8) and for an estimation of penetration depth (Equation 5). This model has been validated over a wide range of speed and laser power, different materials, and different lasers (Lankalapalli, Tu, and Gartner, 1996; Paleocrassas and Tu, 2007), as shown in the next section.

3.2 Model Validation through High Speed Welding of SUS 304

Several SUS 304 specimens, 300 microns thick, were welded at relatively high speeds (200—1000 mm/s) (Miyamoto, *et al.*, 2003). In order to determine the operating Péclet number, apart from the welding speed and the thermal diffusivity, the keyhole radius is also required. Determining the keyhole radius is not trivial. There exists a method (Lankalapalli, Tu, and Gartner, 1996) to estimate the Péclet number from the weld width. The idea is that a contour plot of isotherms can be generated for specific Péclet numbers for the top surface using Equation 8 , and by measuring the width of the curve corresponding to the melting temperature range, the normalized weld width (w/a) and Péclet number can be correlated.

The normalized weld width is obtained by taking twice the maximum y value (due to symmetry) of the melting temperature isotherm curve. Therefore, an equation can be calculated numerically which can be used to determine the Péclet number at the surface of the specimen, for a corresponding weld width.

Figure 4 shows the model prediction compared to the experimental results from Miyamoto et al (2003). The model predicts a satisfactory trend of penetration change versus the Péclet number for different laser powers. However, the data of a specific laser power usually match the predictions of a lower laser power. For example, the data of 170 W laser power match the predictions of 130 W laser power, data of 130 W match better with prediction at 90 W, etc. Based on this observation, it can be stated that approximately 70-80% of laser power is absorbed. This absorption is relatively low, likely due to the very high welding speed.

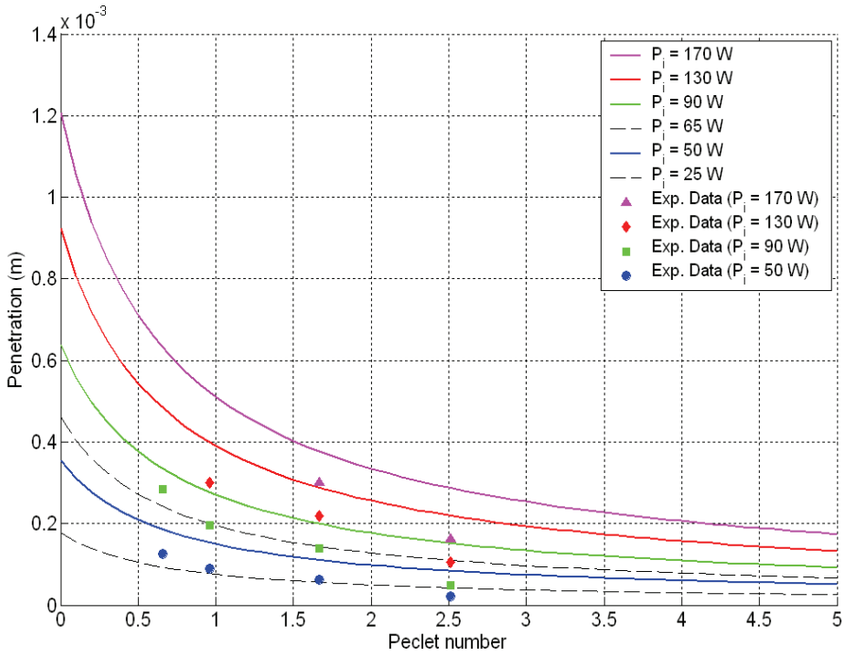

Fig. 4. Theoretical estimate vs. experimentally measured penetration depth in SUS 304.

3.3 Model validation using low speed welding of AA 7075-T6

Figure 5 presents the data/simulation comparison based on the same model for low speed welding of AA7075-T6. As in Figure 4, the model predicts a satisfactory trend of penetration versus the Péclet number. The laser beam absorption is about 90% for welding speeds from 2 mm/s to 10 mm/s. Note that Figures 4 and 5 cover a wide range of Péclet numbers (from 0.5 to 2.5 in Figure 4 and 0.001 to 0.08 in Figure 5). The absorption in Figure 5 is higher than those in Figure 4, likely due to slower welding speed and deeper penetration even though stainless steel is used in Figure 4, while aluminium is used in Figure 5. Once keyhole is formed, the laser beam is absorbed efficiently. For those conditions in Figure 4 with very high welding speeds, the keyhole is shallower and likely tilted to reflect beam power (Fabbro and Chouf, 2000).

However, the point corresponding to 1 mm/s shows a significant decrease in penetration, with its absorbed power being only 68% of the input power. Also, by observing the cross-

sections of the welds at three different processing speeds, it can be seen that the 1 mm/s weld is significantly different from the other two. The 1 mm/s weld shows a significant decrease in aspect ratio. In some cross-sections, large blowholes and porosities were present. The other two welds show more of a conical shaped cross-section, a higher aspect ratio and the absence of any major defects.

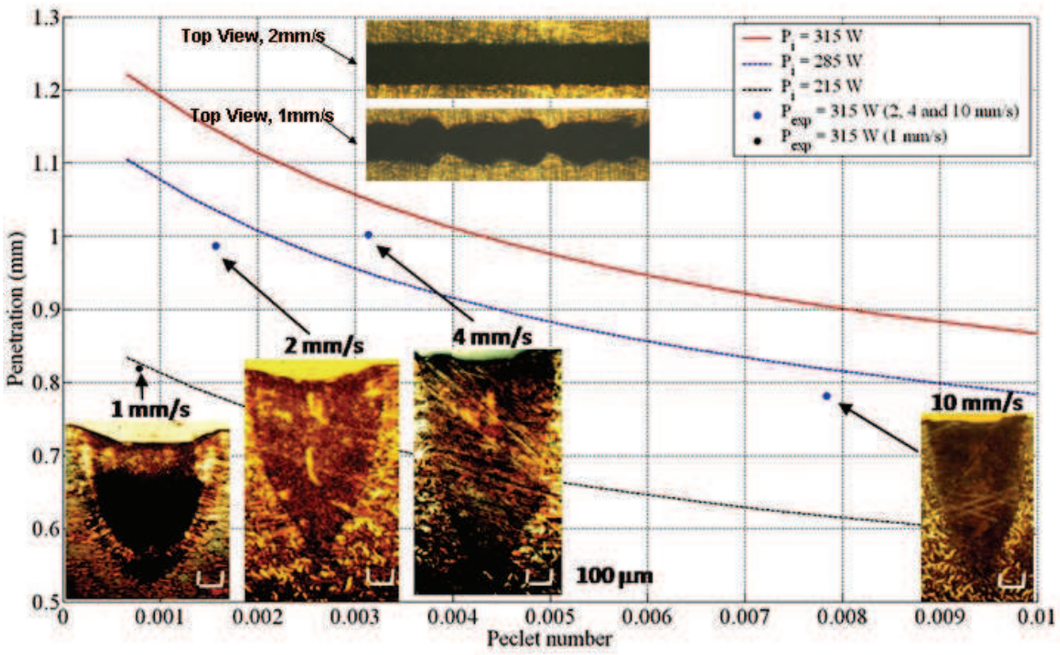

Fig. 5. Model validation for low speed welding of AA 7075-T6

This observation leads to the suspicion that at extremely low speeds the process breaks down and the laser energy is not coupled as efficiently. If this is the case, the model no longer applies to speeds below 2 mm/s.

3.4 Effect of Focusing Positions on Low Speed Welding

Figure 6 shows the change in weld penetration as the focusing position changes (positive indicating the beam is focused into the workpiece).

The general trend is that the best focus position corresponds with the maximum weld depth. This goes along with the recommendation for most welding processes, which is that the focus should be positioned at the desired weld depth (Steen, 2003). Another observation that can be made is that, as the beam is focused past the maximum depth location, the penetration drops at a much higher rate, with the exception of the 10 mm/s condition. This is an indication that the slower speeds are much more sensitive to focusing changes, which means that higher focusing is required to produce adequate and repeatable weld penetrations.

Specifically, for the 10 mm/s processing speed, the maximum weld penetration is approximately both ~ 0.8 mm and this occurs when the focus is approximately 0.9 mm into the workpiece. For the 2 and 4 mm/s speeds the weld penetration is deepest (~ 1 mm) when

the beam is focused approximately 1 mm into the workpiece. The difference in weld penetration (~ 0.8 mm) between these two speeds is not much, with the 4 mm/s weld being slightly deeper. However, the 1 mm/s welds show a significant drop in penetration.

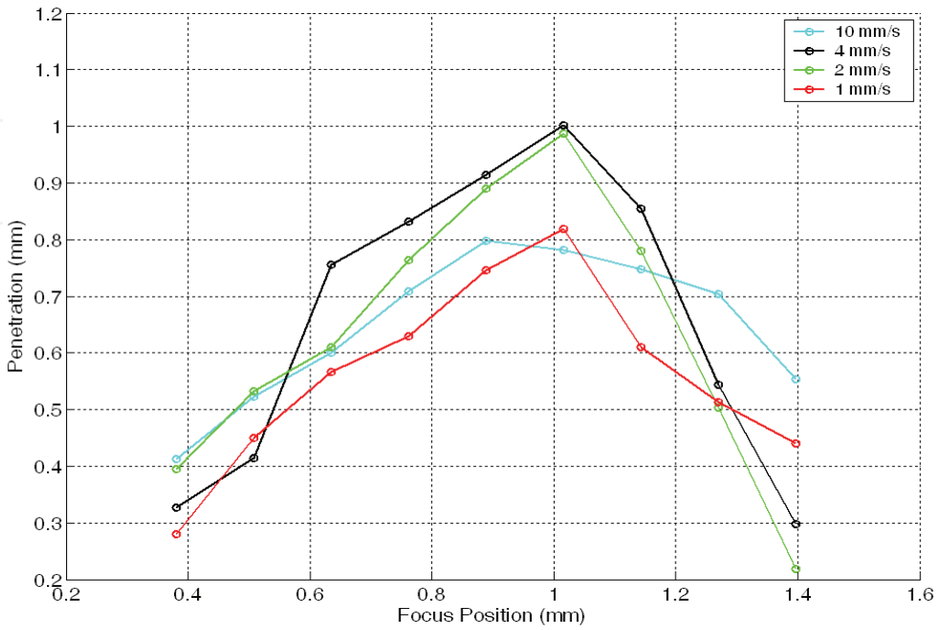

Fig. 6. Effects of focusing position on penetration for different welding speeds.

3.5 Energy-Based Process Characterization

Paleocrassas and Tu (2007) proposed metrics to characterize welding process efficiency. One such metric was defined as keyhole fluence per weld length (KF) which has since been slightly modified and is redefined as follows:

$$\mathrm{KF} = \frac{P_i}{A_b} \cdot \frac{l_w}{v} \cdot \frac{1}{l_w} = \frac{P_i}{A_b \cdot v} \tag{9}$$

where P_i is total incident power, A_b is the outer surface area of the immersed laser beam (as calculated from the beam profile approximation, also shown in Figure 8.7), l_w is the length of the weld and v is the processing velocity. This metric represents the total irradiated energy density per weld length.

As mentioned before, due to different types of power losses during welding, the total irradiated energy density per weld length (KF) from the laser is not going to be completely absorbed by the material. Therefore it is of interest to determine the "weld efficiency" by looking at the total energy used to create the weld and how "well" it is used; for example, the same amount of absorbed weld energy could translate into a shallow and wide weld, or a deep and narrow weld.

Specific weld energy per weld length was also defined by Equation 10 to define how well the amount of energy that used to created the weld was used. In this paper, this metric is denoted as Effective Weld Energy (EWE):

$$\mathrm{E}WE = \frac{m_{weld} \cdot \zeta}{\pi \cdot r_{profile}^2} = \frac{\rho \cdot V_{weld} \cdot \zeta}{\pi \cdot r_{profile}^2} = \frac{\rho \cdot A_{weld} \cdot \zeta}{\pi \cdot r_{profile}^2} \tag{10}$$

where m_{weld}, V_{weld}, A_{weld}, and $r_{profile}$ are the mass, volume and radius of the top profile (or half of the weld width) of the weld (Figure 7), respectively, ρ is the density and ζ is the specific energy of AA 7075-T6, which is determined by

$$\zeta = C_p \cdot \Delta T + \text{Latent Heat of Fusion} \tag{11}$$

where C_p is the specific heat capacity and ΔT is the temperature change between ambient temperature and the melting point.

Figure 8 was generated by applying the above energy based process characterization to the experimental data. The EWE of each data point is plotted with respect to the input KF. There are four sets of data and each set is connected by a different colored line, corresponding to a different processing speed. The 1, 2, 4 and 10 mm/s data are shown in red, green, black and cyan, respectively. Each data point in each set corresponds to a weld created with a different focusing position. The number next to each data point represents how deep the beam is focused into the workpiece, in thousands of an inch. The first observation that can be made is that for each processing speed, the point that has the highest EWE is the one where the beam was focused at approximately 1 mm (.040 in.) into the workpiece, which indicates that it is the focusing condition that produces the best energy coupling. This is the case because the majority of the vapor pressure used to maintain a certain depth is created at the bottom of the keyhole.

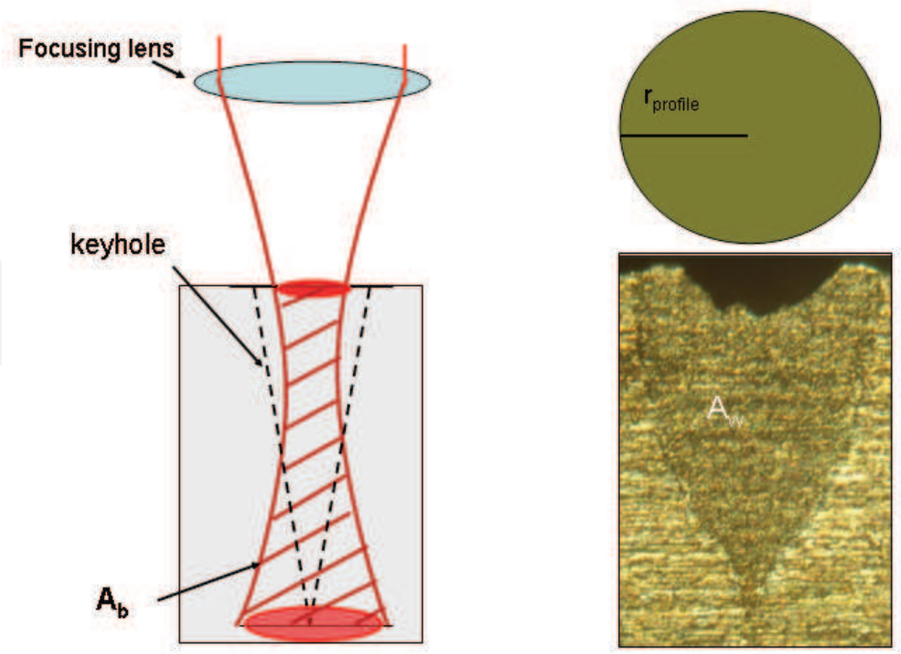

Fig. 7. Schematics showing the submerged beam surface area (A_b), the weld's cross-sectional area (A_w) and the profile radius ($r_{profile}$)

Therefore, placing the focus at the desired weld depth ensures that the maximum power density will be at the bottom of the keyhole, creating the majority of the metal vapor. However, focusing too deep can have an adverse effect on EWE because a minimum power density at the surface is required to create and maintain vaporization of the metal. This explains why the EWE decreases when the laser beam is focused too deep.

By examining the processing speed trend, it was observed that as the speed decreases, the EWE increases, until the speed drops below 2 mm/s. It can therefore be seen that the process is not only dependent on the amount of KF, but also in the manner it is deposited into the workpiece. This leads to the examination of the efficiency of the process.

Global Efficiency: One of the primary concerns in any process involving energy exchange is how efficient it is; in this case, that is, how much of the irradiated energy density per weld length was translated into a desirable, high aspect ratio weld. This is where we can define the "global efficiency" of the process. It is simply the ratio between EWE and KF, as stated in Equation 12.

$$\text{Global Efficiency} = \frac{EWE}{KF} \tag{12}$$

With this metric, we can determine the efficiency at each speed and at each focusing position. If we look at the actual percentages, we will see that the highest efficiency does not exceed 3 percent of the total KF. This might seem extremely low at first, but it is important to remember that this number corresponds only to the energy used to create the weld itself.

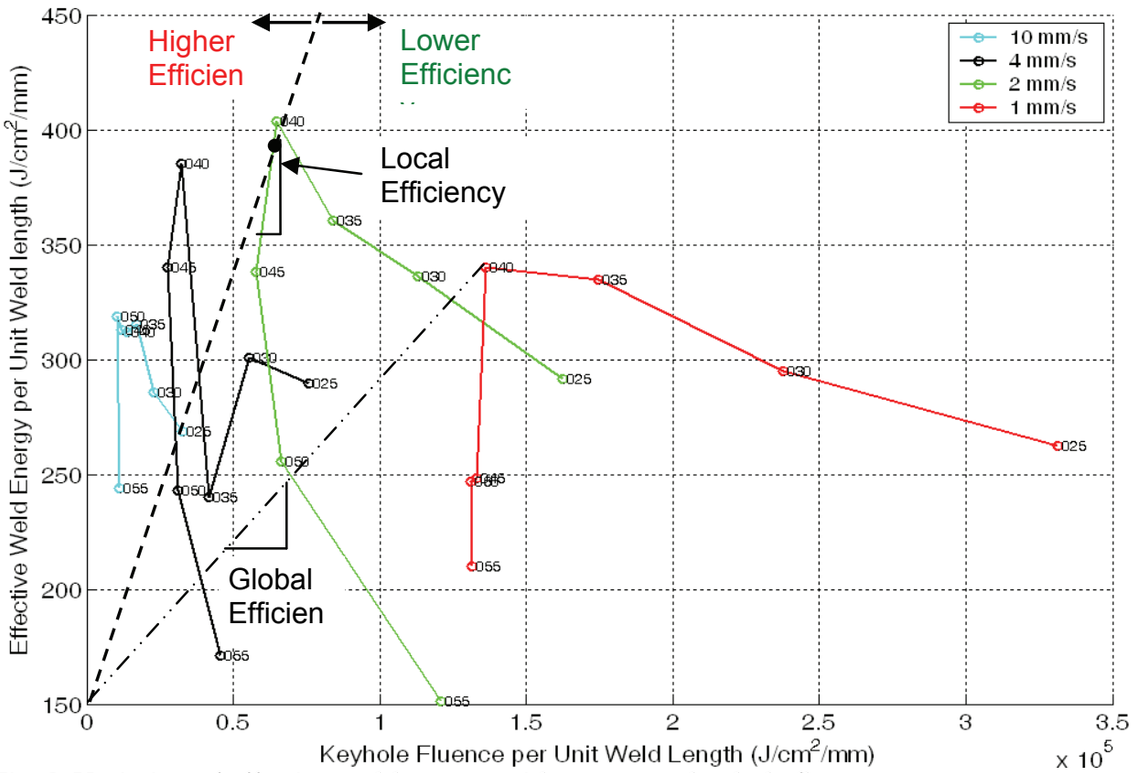

Fig. 8. Variation of effective weld energy with respect to keyhole fluence

During the process, a substantial portion of the absorbed power is conducted away. Therefore the relative change in global efficiency is of more interest than the actual number itself. Looking at the four speeds we observe that the global efficiency decreases slightly from the 10 mm/s data to the 4 mm/s and then slightly lower to 2 mm/s, but drops significantly at the 1 mm/s data. This is another indication that even though there is an increase in KF, the energy is not used as effectively to create a deep and narrow weld. This phenomenon, i.e. the process breakdown of laser welding at extremely low speeds, requires further investigation to explain the reasons behind this drastic change.

Local Efficiency: Another metric we can define to measure the efficiency between different focusing points for a specific processing speed is the "local efficiency." The slopes of these lines can be defined as a "local efficiency" which signifies how efficient the process is, as the focusing changes and the KF increases. In other words it is the ratio of the change in EWE and the change in KF for a particular processing speed (Equation 13).

$$\text{Local Efficiency} = \frac{dEWE}{dKF} \tag{13}$$

It is apparent that the local efficiency is only positive between the weld with the best focusing position and the one that is focused slightly deeper. Again, this is evidence that increasing the KF is not enough to create a good weld, it has to be deposited correctly. It seems that this happens because, when the beam is focused too deep, the incident power density at the surface of the workpiece is not sufficient to create enough vaporization to sustain a keyhole. The process, therefore, switches to conduction welding mode, where a weld is created solely from melting, resulting in a shallow and wide weld. Conversely, if the focus is too close to the surface of the workpiece, the process is again inefficient because the power density at the bottom of the keyhole is too low and cannot sustain the vaporization required for a deeper keyhole.

4. Inherent Process Instability

Table (2) lists the EWEs, global efficiencies, and power efficiencies for the data shown in Figure (8). They clearly showed that the welding became less efficient (from 2.25 % to 0.25 % as the speed drops from 10 mm/s to 1 mm/s) and the quality and aspect ratio of the weld started deteriorating after the processing speed was decreased below 2 mm/s. Large porosities were observed in these very low speed welds in aluminium. This phenomenon is denoted as inherent process instability. In the following sections, the potential contributors of this instability are examined.

Speed (mm/s)	EWE (J/mm^3)	Power Efficiency	"Global" Efficiency
10	312.0	~ 90 %	~ 2.25 %
4	385.0	~ 90 %	~ 1.19 %
2	403.4	~ 90 %	~ 0.62 %
1	340.0	~ 68 %	~ 0.25 %

Table 2. Decrease in EWE and efficiency when speed drops to 1 mm/s.

4.1 Laser Power Distribution

Assuming the laser welding process reaches a quasi-steady state condition, the power distribution, rather than energy distribution, is used to break down the laser power into several components:

$$P_{in} = P_{weld} + P_{cond} + P_{evap} + P_{ref} + (1-\alpha)\cdot P_{vap/plasma} + P_{scat} \tag{14}$$

where P_{in} is the input power from the laser radiation, P_{weld} is the power used to form the weld similar to the definition of EWE, P_{cond} is the power absorbed by the workpiece and then conducted away into the bulk material, P_{evap} is the power absorbed to produce vapor/plasma, P_{ref} is the power reflected away by the workpiece, $P_{vap/plasma}$ is the power absorbed by the vapor/plasma plume hovering above the workpiece, P_{scat} is the power which is scattered away by the vapor/plasma, and α is the fraction of the power absorbed by the vapor/plasma that is re-radiated on the workpiece and absorbed by the workpiece.

All six terms on the right hand side of Equation 14 are unknown. No attempt is made to solve this equation or to measure each of these unknowns precisely. Dividing both sides by P_{in}, Equation 14 becomes

$$1 = \frac{P_{weld}}{P_{in}} + \frac{P_{cond}}{P_{in}} + \frac{P_{evap}}{P_{in}} + \frac{P_{ref}}{P_{in}} + \frac{(1-\alpha)\quad P_{vap/plasma}}{P_{in}} + \frac{P_{scat}}{P_{in}} \tag{15}$$

Each term on the right-hand side of Equation 15 represents the respective percentage of the laser input power. Based on Table (2), it has been confirmed that P_{weld}/P_{in} drops significantly, which should result in changes in some of the rest of the five terms. Therefore, instead of determining the precise value of each term in Equation 15, the attempt is made to determine how the rest of the five terms change as the welding speed drops from 10 mm/s to 1 mm/s.

4.2 Laser Beam Reflectivity Measurements

Among those losses in Equation 14, we first investigate the reflective loss, P_{ref}, to determine if it is a major factor to cause process instability.

Figure (9) shows the reflected laser beam measured by a photodiode at different welding speeds. For each test, the laser beam is first irradiated at the target, remaining stationary for 5 seconds, before actual welding started at speeds from 10 mm/s to 1 mm/s. In every plot, during this 5 second duration in the beginning of the process, there is a large, sudden increase in intensity which gradually dies off to almost a zero state. The substantial reflected laser radiation in the beginning is due to the beam being reflected by the flat surface of the workpiece. As a keyhole forms, the laser beam penetrates deeper into the workpiece and eventually is absorbed by multiple reflections by the keyhole wall. As a deep keyhole acts like a black body, trapping nearly 100 percent of the laser beam, no reflected laser radiation is detected after about 2 seconds, when the keyhole becomes deep enough. After 5 seconds have passed, the workpiece is then translated at the specified welding speed.

When the workpiece begins to move, the reflected signal appears, again, as a series of high frequency spikes, but with a low average intensity, between 0.25 and 0.4 (a.u.). This is pretty

common for processing speeds 10, 4 and 2 mm/s. The spikes in the signals can be attributed to the fact that when the laser beam moves over a solid front, the reflectivity suddenly increases; as soon as that happens, the keyhole is created and it absorbs the beam completely, which causes a decrease in measured intensity. This pattern repeats at a frequency of approximately 30 Hz.

The 1 mm/s processing speed shows a significantly different type of reflected signal, where the spikes are not as strong, but the average intensity of its signal was significantly larger than the other processing conditions' signals, namely approximately 1.4 (a.u.).

On the other hand, when the processing speed is 1 mm/s, the beam does not necessarily move over a solid front, since the molten pool is large. This causes a reduction in the strength of the spikes, because the molten metal has a higher absorptivity than the solid. The increase in average intensity can be explained by the fact that the keyhole is much shallower and wider. Therefore, much more of the laser beam is reflected back, due to the inability of the shallow keyhole to "trap" the laser beam entirely through multiple reflections.

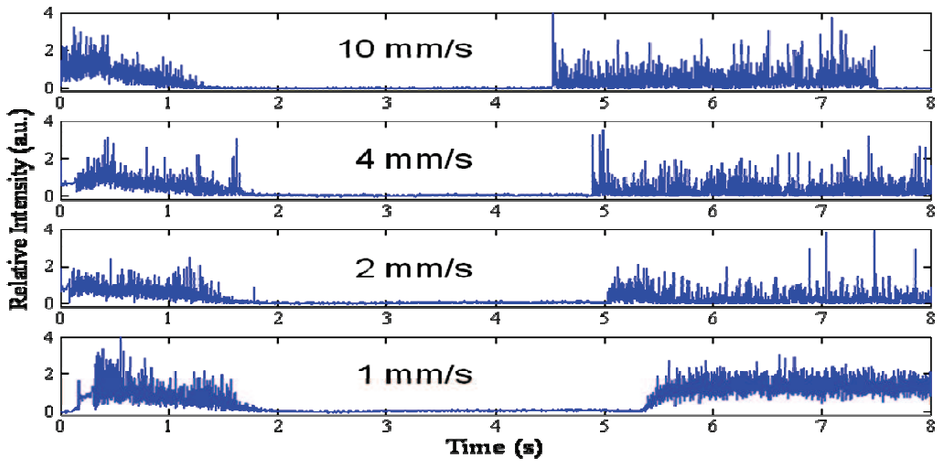

Fig. 9. Measured reflected laser radiations at an angle above the workpiece at different welding speeds.

From Figure (9) it is concluded that the power loss due to reflectivity increases significantly when the speed is lowered down to 1 mm/s. Therefore, the term, P_{ref} / P_{in}, in Equation 15 increases. However, this does not necessarily prove that this increase in reflectivity is the cause of the reduction of P_{weld} / P_{in} in Equation 15.

4.3 Vapor/Plasma Characterization

We conducted a spectroscopic analysis to identify the vapor/plasma effect on the distribution of laser power. The key question is to find out if the vapor/plasma plume, which hovers over the keyhole, is optically "thick" enough to absorb or scatter the laser beam, resulting in reduced laser radiation to reach the work piece. In order to have sufficient signal to noise ratio, we conducted spot welding with a peak power of 1,500 W, which is five times higher than the normal CW welding at 300 W. Even with this much higher peak power, only three Cr I lines (Figure 10) could be detected in the spectroscopic experiment using the Ocean Optics HR4000 spectrometer. Even so, it was deemed

worthwhile to come up with an electron temperature estimation using the Boltzmann plot method. Based on the slope of the fitted line, the resulting temperature estimation is approximately 1,200 degrees Kelvin. This value is well below the vaporization temperature of aluminium (~ 3,275 Kelvin), which indicates that the calculation is not valid. This is probably because the upper energy levels of the measured chromium lines are very close to each other, thus introducing significant errors. Nevertheless, based on this calculation and the fact that the rest of the Cr I lines with higher upper energy levels could not be detected, it is likely that the temperature of the vapor/plasma is fairly low.

To confirm the above finding, we reviewed available literature on the vapor/plasma temperature for Nd:YAG (similar wavelength as fiber laser) laser welding of aluminium alloys. Kim and Matsunawa (1996) used a pulse shapeable YAG laser with irradiations of up to 1 MW/cm^2 on 5000 series aluminium alloys and determined that the vapor/plasma plume was very weakly ionized, with approximate temperatures around 3280 K (barely above the vaporization temperature of aluminium) and electron densities of approximately $1.85 \cdot 10^{13}$ cm^{-3}. Kim et al. (2004) did a similar study and found similar results for even higher irradiations (~ 32 MW/ cm^2), namely the vapor/plasma temperature was very close to the boiling point of aluminium.

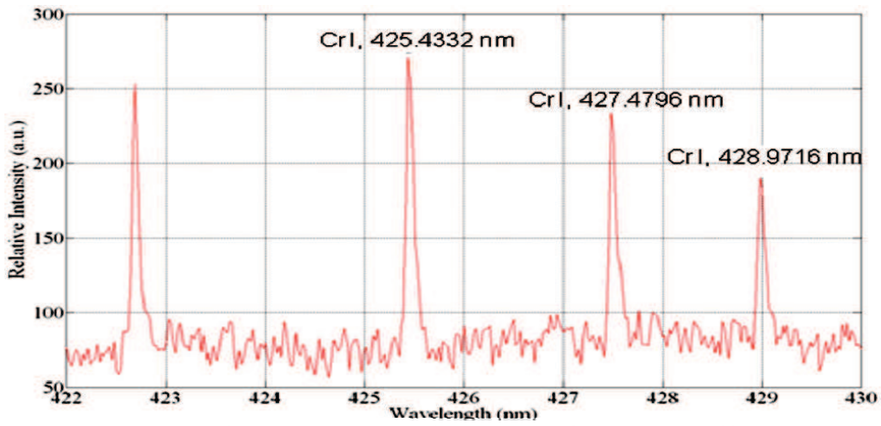

Fig. 10. Aluminium vapor/plasma spectrum for 1 ms pulsing at 100 % power (peak power ~ 1,500 W).

Another group (Lenk et al., 1996) experimented with a Q-switched Nd:YAG laser, operating at power densities of 300 MW/ cm^2, determined electron temperatures of approximately 14,000 K and electron densities of $3 \cdot 10^{16}$ cm^{-3}, and concluded that they "are not high enough for significant absorption by inverse bremsstrahlung." There have been several other studies (Barthélemy et al., 2005, Lu et al., 1999, Knudtson et al., 1987) that have found electron temperatures ranging from 5,000-15,000 K and electron densities up to the order of 10^{18} cm^{-3}, all reaching the same conclusion, namely that IB absorption is not significant. Therefore, it is reasonable to say that the vapor/plasma can be considered to be optically thin. This leads to the conclusion that the last two terms of Equation 15 are of low values and, therefore, their changes, if any, should not be a major factor in the reduction of P_{weld} / P_{in}. This conclusion is different from CO_2 laser welding in which vapor/plasma can grow larger and hotter, and becomes optically thick for the CO_2 laser beam (Tu et al., 2002 and 2003).

The remaining two terms in Equation 15, P_{cond} / P_{in} and P_{evap} / P_{in}, cannot be identified separately. Their changes are considered in the next section.

4.4 The Probable Cause of Process Instability

One probable cause of the process instability which can contribute to increase in P_{cond} / P_{in} and P_{evap} / P_{in}, resulting in the increase in P_{ref} / P_{in}, is if the laser beam mainly irradiates at the molten pool at very low speeds. The molten pool absorbs a large portion of the beam energy near the surface, subsequently transferring the energy into the bulk material via convection, conduction, and evaporation, increasing both P_{cond} / P_{in} and P_{evap} / P_{in} in Equation 15. Thus, this energy is wasted, as it is not used to create keyhole. As a result, the keyhole may become unstable, leading to un-quasi-static behaviors of the welding process (as seen in the top view of the weld in Figure (1)). Consequently, the welding process becomes inefficient and the welds become shallow, uneven, and wide (Figure (5) and Table (2)). As the weld becomes shallow, the laser beam is more easily reflected, resulting in the increase of P_{ref} / P_{in} in Equation 15. As the speed is further reduced, the excessive energy absorbed by the molten pool can also lead to boiling, resulting in large porosities. Readers are referred to Paleocrassas and Tu (2010) for additional tests to investigate this probable cause of instability.

4.5 Significance of the 1 mm/s Threshold

The above analysis helps explain the phenomenon that occurs when the laser welding processing speed drops below a certain low speed threshold. However, a valid question still remains: "why does the laser welding process break down at the particular speed range of about 1 mm/s?"

When the laser beam first irradiates the solid aluminium, it starts to melt and propagate outward with a certain speed. If the welding speed is less than this melting front speed, the laser would fall behind and irradiate on the molten pool. This speed will decrease non-linearly as the surface area surrounding the molten pool also increases non-linearly and therefore the change in molten pool volume.

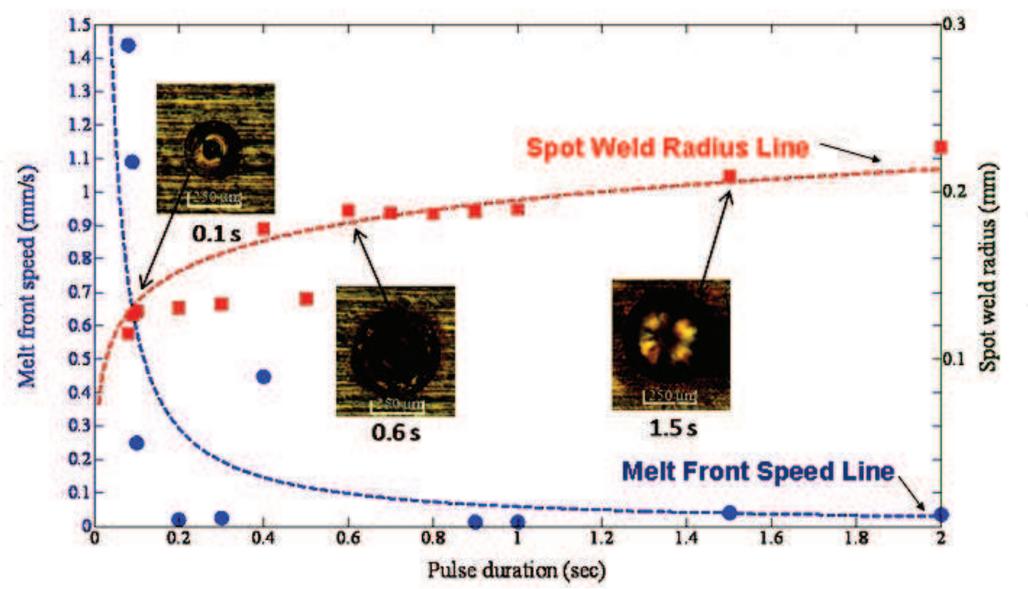

Fig. 11. Change in average melt front speed, as pulse duration is increased

An experiment was conducted to determine the melting front speed. Stationary laser pulses at 100% power, were shot at a AA7075-T6 target with pulse durations ranging from 80 ms to 2000 ms. Figure (11) shows the resulting plot of the melt front speed along with the original data (spot weld radii) for each pulse duration condition.
These melt front speeds are estimated using Equation 16:

$$v_{\text{melt front, i}} = \frac{\left(r_i - r_{i-1}\right)}{\left(t_{p,i} - t_{p,i-1}\right)} \tag{16}$$

where r_i is the radius of the spot weld corresponding to the pulse duration $t_{p,i}$. The first velocity point was calculated by dividing the first spot weld by the corresponding pulse duration. The first spot weld was observed after a laser pulse of 80 ms was irradiated. This was the minimum pulse duration required to produce a spot weld at 300 W (100 %) input power. The speed at which the spot weld formed and propagated was just over 1.4 mm/s.
The experimental results show that from 80 – 90 ms, the melt front speed is estimated to be 1.1 mm/s and for higher pulse durations it drops significantly. The melt front speed at the early stages of molten pool propagation is clearly higher than the 1 mm/s processing speed, which indicates that it initially advances faster than the processing speed. The melt front speed will gradually slow down to a speed below 0.1 mm/s which means that the laser beam will eventually surpass the molten front and irradiate on the solid.
This observation further confirms the fact that at speeds of 1 mm/s or lower, the laser will irradiate directly over the molten pool for a certain period of time, as opposed to the faster processing speeds, which will typically stay slightly ahead of the molten front the whole time. By irradiating over the molten pool the energy will be absorbed more efficiently, further increasing its size and reducing the amount of energy used to maintain keyhole welding.

5. Applications to Aluminium Fatigue Crack Repair

In this section, the low speed laser welding of aluminium is applied to fuse fatigue cracks. There is a serious concern in the aviation industry because airplanes' lifting surfaces undergo millions of cyclic loads throughout their lifetime. After a certain amount of cycles, cracks start to form in the high stress concentration areas. Initially cracks propagate in a stable and predictable manner. After the crack exceeds a certain critical length, it will start growing much faster, in an unstable manner, eventually leading to brittle fracture and catastrophic failure (Sanford, 2003).
Currently, cracks are monitored between flights until they exceed a certain length well below the critical length, after which the cracked part is replaced. This method is very costly due to the loss of flight operation time of the aircraft, as well as the part replacement labor costs.
Reinforcing cracked aluminium structures with composite patches has been recognized as an efficient and economical method to extend the service life of cracked aluminium components (Baker and Jones, 1988; Sun et al, 1996; Daghyani et al, 2003). To further enhance the effectiveness of composite patches, it is envisioned that the crack can be first fused by laser welding to remove the high stress concentration at the crack front before

applying the composite patch (Sun, 2008). The stress intensity factor could be reduced significantly if the fusion is sound.
One challenge is that cracks never propagate in straight lines. This means that the welding speed needs to be reduced and changed in order to trace the crack. Attempts to operate high speed welding would require changing directions abruptly, which will require high accelerations and decelerations. This "jerky" motion in laser welding could lead to inconsistencies in weld width and penetration, thereby compromising the integrity of the weld.
Also, as most of the laser welding experience focused on thick-sheet partial penetration welding, the experience cannot be directly transferred to thin-sheet full penetration welding. In addition, the crack may be skewed across the cross-section of the plate, making it different from welding prepared butt joints.
In this section, the feasibility of the envisioned fusion repair is investigated.

5.1 Cracked Sample Preparation

Fatigue cracks were generated in 2"x 10" thin aluminium sheets (AA7075-T6) with 800 μm thickness using an MTS tensile testing machine. A notch was first machined on one side and then cyclic loads were applied to produce hairline cracks. Depending on the loading, it usually took about 2-3 hours to generate one sample with a 1-1.5" long hairline crack. Care had to taken so that the sample will not crack through and break. Due to the high cost, a total of 20 samples were generated for this study. These hairline cracks were not in straight lines and many of them are skewed across the cross-section as described above.

5.2 Focusing and Workpiece Flatness

Focusing Position: The accepted practice for focusing in thick-sheet partial penetration welding is to focus the beam into the workpiece, without exceeding the maximum penetration that can be achieved for the corresponding power. This is because power density is highest at the focusing plane of the laser beam and by focusing it deep into the material, we can ensure that it will help keep drilling into the molten pool through evaporation of the metal. In the meantime, the power density at the surface of the workpiece should be maintained above the threshold required to melt the solid.
For thin-sheet full penetration conditions, focusing becomes more complicated. If the focus is placed at the bottom surface of the workpiece, violent evaporation may occur, due to the absence of surrounding material to conduct the excess heat away. This may result in a severe disruption of the molten pool, where molten metal gets ejected out of both sides of the workpiece, leading to crude laser cutting rather than laser welding. A similar result will occur if the focus is placed at the top surface of the workpiece. In this case, the best way to focus the laser beam is to create a power density, at the top of the surface, that is just high enough to sustain melting. This will shift the focus to some distance below the workpiece, thereby reducing the power density at the lower surface enough to prevent this violent ejection of the molten pool as well as drop-out.
Flatness Requirement: Because thin sheet aluminium welding is highly sensitive to focusing changes, it is essential to have tight control over the plate's flatness and its position with respect to the laser head. A dial gage was used to check the flatness and the height of the workpiece and a fixture was designed to prevent warping due to thermal distortion during welding.

For thick-sheet, partial penetration welding, changes in focus of about 25-50 μm do not yield significantly different penetration results because the majority of the energy is conducted away and therefore a slight change in power density will not translate into a big percentage of penetration loss.
However, when welding thin-sheets, the slightest increase or decrease in power density could mean the difference between a very violent welding process containing many defects or a weld with insufficient penetration.

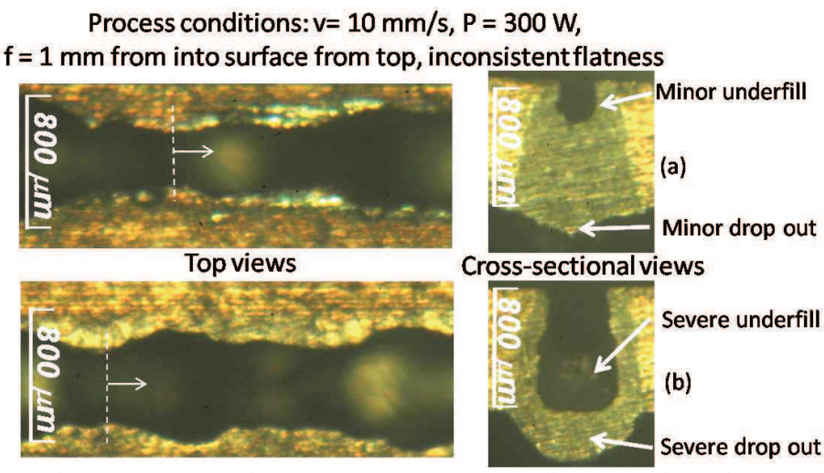

Fig. 12. Top and cross-sectional views of insufficient flatness, thin-sheet, full penetration welds

For example, Figure (12) shows two thin-sheet welds, 1.5 mm apart, on a workpiece with insufficient fixturing. This caused poor flatness, which was about 25 μm for a span of about 50 mm. The resulting welds did not have the desired weld characteristics from beginning to end; namely, consistent width, smooth top and bottom beads and minimal underfill. The welds would start out having the desired consistency and shape and after 20 or 30 millimeters would transition into a violent, unstable process. The welds in Figure (12) show some undesirable characteristics. For both welds, the widths are inconsistent. In Figure (12a) the weld shows a cross-section with minor underfill and drop-out, whereas in Figure (12b) the cross-section reveals significant drop-out and underfill.
Because of this high focusing sensitivity, it is very important that extra care is taken to ensure the flatness of the workpiece is within a tolerance of 10 μm. Also, the relative height between each workpiece needs to be checked to ensure that the focus will lie in the same location. Variations in thickness between workpieces could also interfere with process repeatability if they are larger than the aforementioned tolerance. Due to this high focusing sensitivity, for practical implementation of fusion repair, auto-focusing technology must be used because the structure component may not be flat.

5.3 Crack Tracing

As cracks are not in straight lines, the laser beam must trace the crack precisely. In this study, an off-line method is used for crack tracing. First, the crack sample to be repaired is mounted onto the fixture and a guide beam is used to determine the position coordinates of many points on the crack. A line is then fitted by connecting these points. Usually about 20

to 30 points are identified to trace a crack of 1-1.5" length. This fitted line is then uploaded to the controller of the x-y table for position and welding speed control. Linear motors are used as the driving motors for the x-y table. Figure (13) shows the variation of speed of the x-y table as the crack is being traced.
Once they are finished tracing the crack, the linear motors return to their original positions. We can compare the smoothness of the speed during crack tracing with that of the return, which follows a straight line. The average speed during the crack tracing is 9.34 mm/s and the standard deviation is approximately 2.4 % of the average value. In comparison, during the straight line return the average speed is 9.76 mm/s and the standard deviation is less than 1 % from the average value. Therefore, we can be assured that at 10 mm/s the processing speed stays relatively consistent, without having large deviations during the changes in direction.

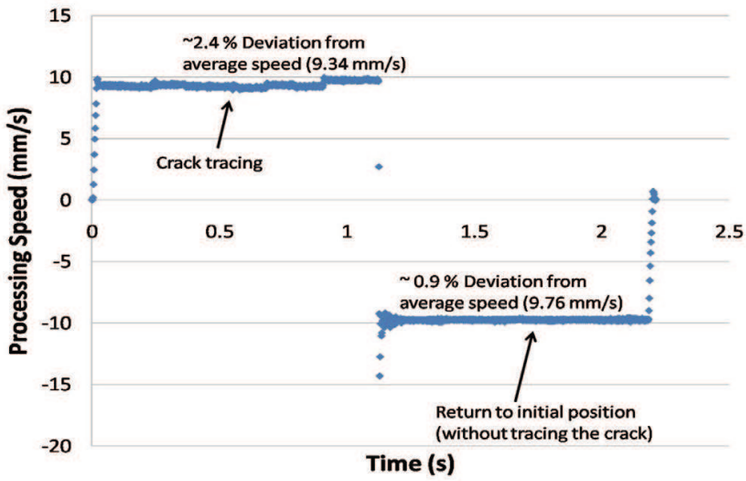

Fig. 13. Variation of the linear motor speed as it traces the crack; comparison with the return of the linear motor to its original position by following a straight line.

5.4 Process Parameter Modification for Thin-Sheet Welding

The first step in transitioning from thick-sheet, partial penetration, bead-on-plate laser welding to thin-sheet, full penetration crack repair, is to find out what parameters combination will yield the best weld results. Several bead-on-plate experiments were performed with the topics discussed in Section 5.2 in mind. The final process parameters are summarized in Table 3.
Initially, the partial penetration welding process parameters were selected as a starting point. Since the transferred welding conditions yielded results resembling laser cutting, it made the most sense to first increase the distance between the nozzle and the workpiece. Doing so, would decrease the pressure exerted on the molten pool by the nitrogen gas. This changed the process from resembling laser cutting to laser welding. By raising the nozzle (3 mm from the surface of the workpiece), the pressure applied by the nitrogen gas to the molten pool was reduced significantly, while still maintaining its shielding from the atmosphere.
Also, the inconsistent results (shown in Figure 2) confirmed that thin-sheet, full penetration welding is very sensitive to small changes in flatness and workpiece height. Therefore, the

fixturing method had to be adjusted to improve the flatness tolerance. Since workpiece warping was also a concern, the workpiece was ”sandwiched” between two thicker aluminium plates, containing a rectangular slot in the area where the workpiece was to be welded. Not only did this prevent warping, but it also significantly improved the flatness of the workpiece.

	Thick-Sheet, Partial Penetration	**Thin-Sheet, Full Penetration**
Output mode, Power (Watts)	CW, 300	CW, 300
Focus position from top surface (mm)	1	1.2
Speed (mm/s)	4	10
Nozzle position from top surface (mm)	1	3
Flatness tolerance per 50 mm span (μm)	> 25	> 10

Table 3. Process parameter comparison between thick-sheet, partial penetration and thin-sheet, full penetration laser welding conditions

By ensuring the flatness to be within 10 μm and adjusting the focusing based on the relative height of the workpiece, the resulting welds turned out to be much more consistent from beginning to end and at the ideal focusing position (1.2 mm from the top surface of the workpiece). The ideal focusing position, as opposed to thick-sheet welding, resulted in deeper than the desired weld penetration (800 μm), which would be at the bottom surface of the workpiece. When focused at the bottom surface, the power densities were too high at both, the top and bottom surfaces, causing a violent process and severe underfill.

The speed also had to be changed, because the excess energy led to a larger molten pool, causing larger drop-out. At 10 mm/s, full penetration was achieved with minimal drop-out.

5.5 Crack Repair by Fusion

A single-pass laser welded crack is shown in Figure (14). The weld was created with minimal underfill and drop-out and with a consistent width and defect free weld bead. Double pass crack repairs, offset by 600 μm (center to center), were used to repair significantly skewed cracks that required larger weld width.

5.6 Mechanical Testing for Determining Repaired Crack Strength

Tensile tests were conducted for single and double pass welds, as well as unwelded (baseline) AA 7075-T6 sheets. Both the ductility and the ultimate strength were recorded. The results are shown in Figure (15). Four samples for each condition were tested due to limited numbers of crack samples and due to the fact that the results were highly repeatable (see below).

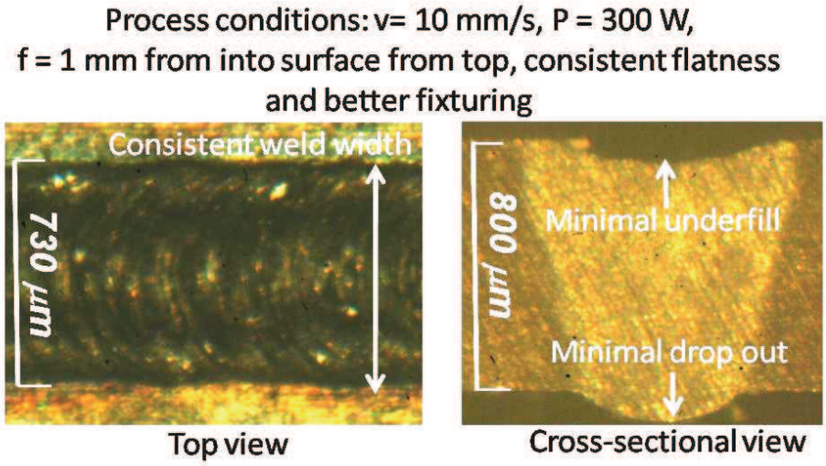

Fig. 14. Single-pass laser welded fatigue crack

The average UTS of the base AA 7075-T6 is 579 MPa, which is identical to the documented value (Sanford, 2003). As shown in figure 7, the lowest strength is 571 MPa and highest is 584 MPa, equivalent to –1.4 % to +0.9% in variation from the average value. The average UTS of the single-pass weld is 430 MPa, which is 74 percent of the base alloy's strength. The lowest is 411 MPa and the highest is 443 MPa, equivalent to –4.4% to +3.0% variation from the average. The average UTS of the double-pass weld is 395 MPa, which is 68 percent of the base alloy's strength. The lowest is 379 MPa and the highest is 422 MPa, equivalent to -4.1% to +6.8 % variation from the average value. These values are extremely encouraging because the UTS for AA 7075-O, which is the same alloy without heat treatment, is only 220 MPa (Sanford, 2003). The single pass weld is 95% higher than that of the untreated alloy, while the double pass weld is 72% higher. These high strength values indicate that the laser did not completely destroy the heat treatment temper. The strength is probably retained due to the use of the fiber laser which, with its highly concentrated energy deposition, produces narrow welds to allow for fast cooling by the bulk material.

As the results of the UTS strength results were highly repeatable, no more samples were tested. For the tensile tests to determine UTS, four samples with highly repeatable results are justified. However, it should be noted that if fatigue life were to be tested, more samples would be needed as fatigue life tests usually exhibits wider statistical distribution. In this study, no attempt was made to test the fatigue life as crack fusion alone should not be considered a viable repair technique unless it is used together with composite patches. It should be clear to see the benefit of the because without it crack fusion, the composite patch is bonded to a part with zero UTS at the crack region and with a high stress intensity factor at the crack front. On the other hand, with crack fusion, the UTS is 172% - 195% that of the untreated alloy and there is no crack front with a high stress concentration.

In addition to tensile tests, the ductility was also measured. The average elongation for the base alloy was measured to be 4.9 percent, while the single pass weld was just under 1 percent and the double bead-on-plate was approximately 0.5 percent. The significant drop in ductility was probably due to the rapid cooling of the weld as described earlier. For the double-pass weld, the second pass re-melted some weld of the first pass, which probably caused the ductility to drop even further. This effect has been observed before (Verkat et al.,

1997) in laser welding and can be improved slightly with the appropriate addition of filler wire (Yoon and Wallach, 2008).

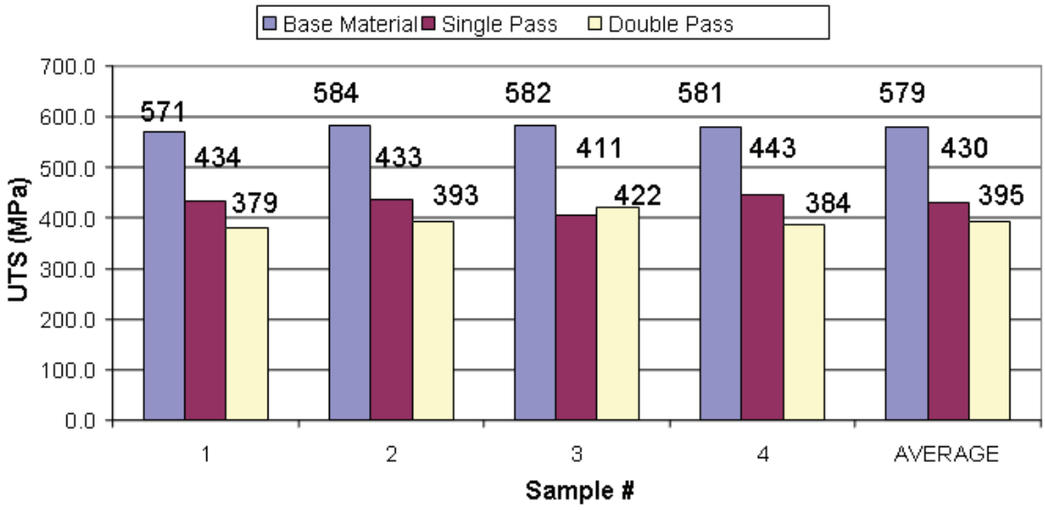

Fig. 15. Base AA 7075-T6 compared to single and double pass bead-on-plate welds

6. Conclusion

In this chapter, topics related to extending fiber laser welding of aluminium in the low speed range were discussed. General topics, such as the properties of aluminium and welding defects, review of high speed laser welding of aluminium, and fiber laser characteristics and optical setups for safety, were first reviewed. Recent research results on the modelling and validation of laser welding of aluminium, experimental characterization of low speed welding processes, and the instability phenomenon and its probable causes were then presented. Finally, an application of low speed fiber laser welding of aluminium for repairing fatigue cracks was discussed.

The difficulty in extending fiber laser welding of aluminium to low speeds is that there exists a low speed threshold (1 mm/s), below which the process becomes unstable. This threshold appears to be related to the molting front propagation speed, which was found to be approximately 1.1 – 1.4 mm/s. Therefore, when the welding speed is less than 1 mm/s, the laser irradiates over the molten pool longer, resulting in less efficient energy coupling for forming high aspect ratio welds. One possible solution to avoid this problem is to employ pulsed welding to reduce the laser power when it is irradiating over the molten pool and to resume the laser power when it moves over a solid surface. More research is needed to devise suitable pulsing schemes based on this instability observation.

Additionally, more studies are needed to understand the overheating of the molten pool and the keyhole stability, as well as the keyhole's interaction with the melting front. It is also important to study how the laser energy density and the currently observed low speed threshold, 1 mm/s, are related. It would be useful to devise new experiments to quantify each term in Equation 14 to further understand the overheating of molten pool.

Finally, the most challenging factor for successful crack fusion is related to the plate flatness which critically affects the relative position between the laser focusing point and the plate

location. It has been found that the plate flatness needs to be maintained to be within +- 10 μm for the welding process to be consistent. In practical implementation, an auto-focus system must be developed to maintain proper focusing so that crack fusion can be achieved even for curved plates. Another important technical difficulty is related to crack tracing. An automatic crack tracing system needs to be developed for practical implementation.

7. References

Allen, C. M., Verhaeghe, G., Hilton, P. A., Heason, C.P., Prangnell, P.B. (2006) Laser and hybrid laser-MIG welding of 6.35 and 12.7mm thick aluminium aerospace alloy. *Materials Science Forum*, 519-521, (2), pp.1139-1144.

Baker, A.A. and Jones, R. (1988) *Bonded repair of aircarft structures*, Martinus Nijhoff Publishers.

Barthélemy, O., Margot, J., Chaker, M., Sabsabi, M, Vidal, F., Johnston, T.W., Laville, S., Le Drogoff, B. (2005) Influence of the laser parameters on the space and time characteristics of an aluminium laser-induced plasma. *Spectrochimica Acta Part B*, 60, pp. 905-914.

Brown, R. T. (2008) Keyhole welding studies with a moderate-power, high brightness fiber laser. *Journal of Laser Applications*, 20 (4), pp. 201-208.

Cao, X., Wallace, W., Immarigeon, J.-P., and Poon, C. (2003a) Research in laser welding of wrought aluminium alloys. I. laser welding processes. *Materials and Manufacturing Processes*, 18(1), pp. 1-22.

Cao, X., Wallace, W., Immarigeon, J.-P., and Poon, C. (2003b) Research in laser welding of wrought aluminium alloys. II. metallurgical microstructures, defects, and mechanical properties. *Materials and Manufacturing Processes*, 18 (1), pp. 23-49.

Carslaw, H. S., Jaeger, J. C. (1962) *Conduction of Heat in Solids*, 2nd edition, Oxford: Clarendon, pp. 390.

Cieslak, M. J. (1992) Phase transformations in weldments: new materials and new perspectives. *3rd Int. Conf. on Trends in Welding Research*, Gatlingburg, TN, pp. 229.

Dausinger, F., Rapp, J., Beck, M., Faisst, Hack, R., Hugel, H. (1996) Welding of aluminium: a challenging opportunity for laser technology. *Journal of Laser Applications*, 8, pp. 285-290.

Dausinger, F., Rapp, J., Hohenberger, B., Hugel, H. (1997) Laser beam welding of aluminium alloys: state of the art and recent developments. *Proc. Int. Body Engineering Conf. IBEC '97: Advanced Technologies & Processes*, 33, pp. 38-46.

Daghyani, H.R., Sayadi, A., and Hosseini Toudeshky, H. (2003) Fatigue crack propagation of aluminium panels repaired with adhesively bonded composite laminates. *Proceedings of the institution of Mechanical Engineers, Part L: Journal of Materials: Design and Applications*, pp. 291-293.

Duley, W. W. (1999) *Laser Welding*, 1st edition, John Wiley & Sons, Inc., pp. 4-65.

Freudenstein, S., Cooper, J. (1979) Stark broadening of Fe I 5383 Å. *Astron. Astrophys*., 71. pp. 283-288.

Fabbro, R. and Chouf, K. (2000) Dynamical description of the keyhole in deep penetration laser welding. *Journal of Laser Applications*, 12 (4), pp. 142-148.

Industrial Laser Solutions (2005)Jan.

Ion, J. C. (2000) Laser beam welding of wrought aluminium alloys. *Sci. Technol. Weld. Joining*, 5 (5), pp. 265-276.

IPG, Inc. (2003) 300W single-model fiber laser operation manual.

Katayama, S., Mizutani, M. (2002) Laser weldability of aluminium alloys. *Trans. JWRI*, 31 (2), pp. 147-155.

Katayama, S., Mizutani, M., Matsunawa, A. (2003) Development of porosity prevention procedures during laser welding. *Proc. of SPIE*, 4831, pp. 281-288.

Katayama, S., Nagayama, H., Mizutani, M., Kawahito, Y. (2008) Fiber laser welding of aluminium alloy. *Keikinzoku Yosetsu/J. of Light Metal Welding and Construction*, 46 (10), pp. 34-43.

Kim, J.D. and Matsunawa, A. (1996) Plasma analysis in laser welding of aluminium alloys. *International Institute of Welding*, pp. 1-9.

Kim, J.D., Oh, J.S., Lee, M.H., Kim, Y.S. (2004) Spectroscopic analysis of plasma induced in laser welding of aluminium alloys. *Material Science Forum*, 449-452, pp. 429-432.

Knudtson, J.T., Green, W.B., Sutton, D.G. (1987) The UV-visible spectroscopy of laser produced aluminium plasmas. *J. Appl. Phys.*, 61 (10), pp. 4471-4780.

Kutsuna, M., Yan, Q. U. (1998) Study on porosity formation in laser welds of aluminium alloys (Report 2). mechanism of porosity formation by hydrogen and magnesium. *J. Light Met. Weld. Constr.*, 36 (11), pp. 1-17.

Lankalapalli, K. N., Tu, J. F., Gartner, M. (1996) A model for estimating penetration depth of laser welding processes. *J. Phys. D, Appl. Phys.*, 29, pp. 1831-1841.

Lenk, A., Witke, T., Granse, G. (1996) Density and electron temperature of laser induced plasma – a comparison of different investigation methods. *Applied Surface Science*, 96-98, pp. 195-198.

Lu, Y.F., Tao, Z.B., Hong, M.H. (1999) Characteristics of excimer laser induced plasma from an aluminium Target by spectroscopic study. *Jpn. J. Appl. Phys*, 38, pp. 2958-2963.

Mandal, N. R., 2002, Aluminium Welding, 1st edition, Narosa Publishing House, pp. 1-19 Martukanitz, R. P., Smith, D. J. (1995) Laser beam welding of aluminium alloys. *Proc 6th Int. Conf. on Aluminium Weldments, AWS*, pp. 309-323.

Matsunawa, A. (1994) Defects formation mechanisms in laser welding and their suppression methods. *Proc. of ICALEO*, pp. 203-219.

Matsunawa, A., Katayama, S., Fujita, Y. (1998) Laser welding of aluminium alloys— defects formation mechanisms and their suppression methods. *Proc. 7th Int. conf./INALCO '98: Joints in Aluminium*, Cambridge, pp. 65-76.

Miyamoto, I., Park, S.-J., Ooie, T. (2003) Ultrafine-keyhole welding process using single-mode fiber laser. *Proc. of ICALEO*: 203-212.

Molian, A. (2004) Private conversation.

Naeem, M and Lewis, S. (2006) Micro joining and cutting with a single mode fiber laser. *Proc. of PICALO*, pp. 400-405.

Oi, J.F., Tian, S., Chen, H., Xiao, R.S., Zuo, T.C. (2006) Slab CO_2 laser welding of 7075-T6 high strength aluminium alloy. *Zhongguo Jiguang/Chinese J. of Lasers*, 33 (SUPPL). pp. 439-444.

Paleocrassas, A.G. and Tu, J.F. (2007) Low-speed laser welding of aluminium alloy 7075-T6 using a 300-W, single-mode, ytterbium fiber laser. *Welding Journal*, 86 (6), pp. 179.s-186.s.

Paleocrassas, A.G. and Tu, J.F. (2010) Inherent instability investigation for low speed laser welding of aluminium using a single-mode fiber laser. *J. Material Processing Technology*, doi:10.1016/j.jamatprotec2010.04.002.

Poueyo-Verwaerde, A., de Frutos, A.M., Orza, J.M. (1993) Experimental study of laser induced plasma in welding conditions with continuous CO_2 laser. *J. Appl. Phys*. 74 (9), pp. 5773-5780.

Ramasamy, S., Albright, C. E. (2000) CO_2 and Nd:YAG laser beam welding of 6111-T4 aluminium alloy for automotive applications. *J. of Laser Appl*., 12 (3), pp. 101-115.

Salminen, A. S., Kujanpaa, V. P., Moisio, T. J. I. (1994) Effect of use of filler wire on requirements of laser welded butt joints. *Proc. of ICALEO*: 193-202.

Sanford, R.J. (2003) *Principles of Fracture Mechanics*, 1st edition, Prentic Hall, pp. 386-387.

Steen, W. M. (2003) *Laser Material Processing*, 3rd edition, Springer-Verlag London Limited, pp. 61-106.

Sun, C.T., Klug, J., and Arendt, C. (1996) Analysis of cracked aluminium plates repaired with bonded composite patches. *AIAA Journal,* 54, pp. 369-374.

Sun, C.T., School of AAE, Purdue University, 2008, private conversation.

Tu, J.F., Inoue, T., Miyamoto, I. (2003) Quantitative characterization of keyhole absorption mechanisms in 20 kW-class CO_2 laser welding process. *J. Phys. D: Appl. Phys*. 36, pp. 192-203.

Tu, J.F., Miyamoto, I., Inoue, T. (2002) Characterizing keyhole plasma light emission and plasma plume scattering for monitoring 20 kW class CO_2 laser welding processes. *J. Laser Applications*, 14 (3), pp. 146-153.

Venkat, S., Albright, C.E., Ramasamy, S., Hurley (1997) CO_2 laser beam welding of aluminium 5754-O and 6111-T4 alloys. *Welding Journal*, 76(7), pp. 275.s-282.s.

Wagner, F. (2006) Laser beam welding with single mode fibre lasers. *Proc. Of PICALO*, pp. 339-343.

Weeter, L. (1998) Technological advances in aluminium laser welding, *Pract. Weld. Today*, 2 (1), pp.56-58.

Xu, L., Tian, Z., Peng, Y., Xiao, R., Yang, W. (2008) Microstructure and mechanical properties of high strength aluminium alloy laser welds. *Zhongguo Jiguang/Chinese J. of Lasers*, 35 (3), pp. 456-461.

Yoon, J.W., Wallach, E.R. (2008) CW CO_2 laser welding of Al-Mg alloys with filler wires. *Material Science Forum*, 580-582, pp. 539-542.

Yoshikawa, M., Kurosawa, T., Nakata, K., Kimura, S., Aoki, S. (1995) YAG laser welding of aluminium alloys. *Journal of Light Metal Welding & Construction*, 32 (9), pp. 15-23.

Zhao, H., White, D. R., DebRoy, T. (1999) Current issues and problems in laser welding of automotive aluminium alloys. *Int. Mater. Rev*., 44(6), pp. 238-266.

Laser Welding

Edited by Xiaodong Na, Stone

ISBN 978-953-307-129-9

Hard cover, 240 pages

Publisher Sciyo

Published online 17, August, 2010

Published in print edition August, 2010

This book is entitled to laser welding processes. The objective is to introduce relatively established methodologies and techniques which have been studied, developed and applied either in industries or researches. State-of-the art developments aimed at improving or next generation technologies will be presented covering topics such as monitoring, modelling, control, and industrial application. This book is to provide effective solutions to various applications for field engineers and researchers who are interested in laser material processing.

How to reference

In order to correctly reference this scholarly work, feel free to copy and paste the following:

Jay Tu and Alexander Paleocrassas (2010). Low Speed Laser Welding of Aluminium Alloys Using Single-Mode Fiber Lasers, Laser Welding, Xiaodong Na, Stone (Ed.), ISBN: 978-953-307-129-9, InTech, Available from: http://www.intechopen.com/books/laser-welding/low-speed-laser-welding-of-aluminium-alloys-using-single-mode-fiber-lasers

INTECH
open science | open minds

InTech Europe
University Campus STeP Ri
Slavka Krautzeka 83/A
51000 Rijeka, Croatia
Phone: +385 (51) 770 447
Fax: +385 (51) 686 166
www.intechopen.com

InTech China
Unit 405, Office Block, Hotel Equatorial Shanghai
No.65, Yan An Road (West), Shanghai, 200040, China
中国上海市延安西路65号上海国际贵都大饭店办公楼405单元
Phone: +86-21-62489820
Fax: +86-21-62489821

IntechOpen